processes

MDPI

Article

Nickel-Stage Addition in Si-MCM-41 Synthesis for Renewable Hydrogen Production

Lígia Gomes Oliveira [1,2], Cleuciane Tillvitz do Nascimento [1,2], Bárbara Bulhões Cazula [1,2,*], Anabelle Tait [1], Carlos de Jesus de Oliveira [1,2], Guilherme Emanuel Queiros Souza [1,2], Lázaro José Gasparrini [1,2], Áquila de Oliveira Alencar [1], Gabriela Ritter [1], Natália Neumann Jorge [1] and Helton José Alves [1,2]

[1] Laboratory of Materials and Renewable Energy (LABMATER), Department of Engineering and Exact Sciences, Federal University of Paraná—UFPR, 2153 Pioneiro Street, Jardim Dallas, Palotina 85950-000, PR, Brazil; gui.emanuel97@gmail.com (G.E.Q.S.); helquimica@gmail.com (H.J.A.)

[2] Environmental Engineering and Technology Postgraduate Program (PPGETA), Federal University of Paraná—UFPR, 2153 Pioneiro Street, Jardim Dallas, Palotina 85950-000, PR, Brazil

* Correspondence: barbarabulhoes@hotmail.com; Tel.: +55-(44)3211-8500

Abstract: Among the countless routes for renewable hydrogen (H_2) production, Biogas Dry Reforming (DR) has been highlighted as one of the most promising for the circular bio-economy sector. However, DR requires high operating temperatures (700 °C–900 °C), and, for greater efficiency, a thermally stable catalyst is necessary, being, above all, resistant to coke formation, sintering, and sulfur poisoning. Mesoporous metallic catalysts, such as nickel (Ni) supported on silica, stand out due to their high catalytic activity concerning such characteristics. In this regard, the presented work evaluated the influences of the nickel addition stage during the synthesis of mesoporous catalyst type Si-MCM-41. Two different catalysts were prepared: catalyst A (Ni/Si-MCM-41_A), synthesized through the in situ addition of the precursor salt of nickel ($Ni(Ni(NO_3)_2{\cdot}6H_2O$) before the addition of TEOS (Tetraethyl orthosilicate) and after the addition of the directing agent; and catalyst B (Ni/Si-MCM-41_B), resulting from the addition of the precursor salt after the TEOS, following the conventional methodology, by wet impregnation in situ. The results evidenced that the metal addition stage has a direct influence on the mesoporous structure. However, no significant influence was observed on the efficiency concerning BDR, and the conversions into H_2 were 97% and 96% for the Ni/SiMCM-41_A and Ni/Si-MCM-41_B catalysts, respectively.

Keywords: dry reforming of biogas; renewable hydrogen; Ni/Si-MCM-41 catalyst; Ni addition stages

check for updates

Citation: Oliveira, L.G.; do Nascimento, C.T.; Cazula, B.B.; Tait, A.; de Oliveira, C.d.J.; Souza, G.E.Q.; Gasparrini, L.J.; Alencar, Á.d.O.; Ritter, G.; Jorge, N.N.; et al. Nickel-Stage Addition in Si-MCM-41 Synthesis for Renewable Hydrogen Production. *Processes* **2024**, *12*, 1836. https://doi.org/10.3390/pr12091836

Academic Editor: Rafal Gieleciak

Received: 24 July 2024
Revised: 20 August 2024
Accepted: 27 August 2024
Published: 29 August 2024

Copyright: © 2024 by the authors. Licensee MDPI, Basel, Switzerland. This article is an open access article distributed under the terms and conditions of the Creative Commons Attribution (CC BY) license (https://creativecommons.org/licenses/by/4.0/).

1. Introduction

Energy from hydrogen has been widespread worldwide, with production of hydrogen fuel reaching 120 million tons/year, while natural gas and coal are responsible for 95% of H_2 production [1]. This fact, associated with environmental damages caused by greenhouse emissions, contributes hugely to the development of new alternative energy sources with low carbon emissions. Among the technologies with low carbon emissions, the production of renewable H_2 has impelled researchers and governments in many countries due to the benefits of this type of energy, especially for environmental preservation [2]. Hydrogen can be burned to generate energy with water as a by-product and can also be used as a precursor to other reactions, such as Fischer–Tropsch, to produce hydrocarbons (bio-syncrude) [3].

The high demand for renewable hydrogen is directly related to economic and industrial development [4]. This demand for fuels reinforces the decentralization and reduction of CO_x emissions into the atmosphere. Hydrogen production from conventional sources is already used more frequently, as it utilizes more mature technology, such as the use of natural gas and coal gasification [5]; however, these processes emit elevated concentrations of pollutants in addition to the environmental impact caused by the exploration of non-renewable fuels [6]. In this sense, to achieve a sustainable hydrogen economy, it is essential

to advance production methods with less impact on its production, aiming at environmental quality and a considerable quality of life [7]. Additionally, the successful construction of a hydrogen society requires technological advances in terms of production rational design, and the storage, delivery, and use of hydrogen [8,9], as well as the exploration of alternative routes and the consolidated development of processes, accompanied by studies focused on different techniques for obtaining and using hydrogen [10]. Nowadays, hydrogen production through alternative and renewable routes can occur through various technologies, such as biomethane reforming, whether steam, autothermal, or dry reforming, e.g., and mostly by the electrolysis process—associated with a renewable energy source [11].

Concerning the obtaining of renewable methane (CH_4) to add to the hydrogen production route, one of the affecting factors is the origin of the raw material [12]. A promising route is obtaining methane biomass such as food waste, agro-industrial waste, effluents, and any compound rich in organic matter. This process occurs through fermentation and the gas product is composed mainly of methane and carbon dioxide [13]. In this way, biogas (CH_4 and CO) is an important player in renewable hydrogen production in Brazil [14], since the country is rich in biomass for renewable energy, as it has an advantageous territorial extension and an appropriate climate for biogas investments.

Brazil has committed to adding at least 5% of its renewable hydrogen to its gas pipeline networks until 2032, and 10% until 2050. From these numbers, 60% will be obtained from renewable energy sources such as solar, wind, biomass, and biogas; by 2050, the contribution of renewable H_2 is expected to reach 80% [15]. In this way, the search for feedstock and technologies to produce renewable hydrogen on an industrial scale with effectiveness and economic viability has become fundamental within the world energy scenario.

Dry reforming (DR) is an alternative route that can be used to obtain renewable H_2. In this process, methane (CH_4) and carbon dioxide (CO_2), the main constituents of biogas, are converted into syngas ($CH_4 + CO_2 \rightleftharpoons 2CO + 2H_2$) [16,17]. However, DR requires relatively high operating temperatures (700 °C–900 °C) and an efficient and selective heterogeneous catalyst to be advantageous [18]. There has been extensive research in recent years focusing on synthesizing catalysts that are economically and technologically viable, effective, and resistant to coke (carbon) formation, sintering, and sulfur poisoning, for application in reaction systems at high temperatures [19,20].

Ni-based catalysts supported on mesoporous materials with elevated surface areas, such as MCM-41, are a prominent alternative for application in DR [17,21]. Ni offers good selectivity for DR, providing significant conversion rates, and Si-MCM-41 usually allows good metal dispersion on its surface, due to its high chemical and thermal stability [22] Additionally, Ni presents good resistance to sintering and coke formation, and is more cost-effective compared to noble metals such as Pt and Pd. Recent works developed for the research group of [23] studied the use of Ni supported on Si-MCM-41 as the catalyst applied on DR, studying mainly the variation of Ni content on the supports aiming for high H_2 yield production. Also, Cazula et al. [24] evaluated the optimization of the parameter's synthesis of Si-MCM-41, aiming to observe the support influence on Ni-catalysts for DR, achieving high H_2 production, as well.

As far as our search indicates, the effect of the metal addition stage, concerning the catalytic structure construction, has not been reported in associated literature studies. In that regard, evaluating the Ni addition stage, before or after the mesoporous structure formation, helps to understand its influence on surface area and pore diameter parameters, directly influencing the catalyst performance on DR. Therefore, the presented work proposes evaluating the influences of the Ni addition stage during the synthesis of Si-MCM-41 catalysts; studying two different Ni addition stages, in situ, before the addition of TEOS, and after the addition of the directing agent; and by wet impregnation, following the conventional methodology.

2. Experimentation

2.1. Ni/Si-MCM-41 Synthesis

Both Ni catalysts were prepared according to the methodology proposed by Grün et al. (1999) [25]. Nickel (II) nitrate hexahydrate ($Ni(NO_3)_2 \cdot 6H_2O$) was used as the metal precursor and mixed with the Si-MCM-41 support following the steps below. The amount of metallic salt used was calculated based on Equation (1).

$$m_{salt} = \frac{\%_{metal} \cdot m_{support} \cdot MM_{salt}}{MM_{metal} \cdot (100 - \%_{metal})} \quad (1)$$

In which, m_{salt} is the molecular mass of nickel nitrate (g mol^{-1}), $\%_{metal}$ is the mass in percentage of the salt, $m_{support}$ is the support mass (g), MM_{salt} is the molecular mass of the metallic salt (g mol^{-1}), and MM_{metal} is the molecular mass of the metal (g mol^{-1}).

For this study, two types of catalysts, identified as A and B, were synthesized. The Ni stage addition for the synthesis of catalyst A occurred before the silica source (TEOS) step. Meanwhile, in the catalyst B synthesis, Ni was added after the TEOS addition stage.

2.1.1. Synthesis of Catalyst A (Ni/Si-MCM-41_A)

For the synthesis of catalyst A, 128.25 mL of ultrapure water (Milli-Q®), 8.55 g of hexadecyltrimethylammonium bromide (CTAB) (Sigma Aldrich, Barueri, SP, Brazil, 99%), and 28.23 g of nickel nitrate (Neon, Suzano, SP, Brazil, 97%) (mass calculated from Equation (1)) were mixed. The mixture was stirred at 100 rpm for 60 min at 30 °C. Then, 115.65 mL of ammonium hydroxide (Anidrol, Diadema, SP, Brazil, 28–30%) and 120.35 mL of ethanol (Neon, Suzano, SP, Brazil, 99.8%) were added, while maintaining stirring and temperature. After, 17.25 mL of TEOS (Sigma Aldrich, Barueri, SP, Brazil, 98%) was added, and the mixture was stirred for an additional 60 min at 30 °C. The resulting gel was washed with 500 mL of distilled water, vacuum filtered, and oven-dried at 60 °C for 48 h, as adapted from the methodology described by Cazula et al. [26] and Zhuang et al. [27].

2.1.2. Synthesis of Catalyst B (Ni/Si-MCM-41_B)

Catalyst B was synthesized using 128.25 mL of ultrapure water with 8.55 g of CTAB, 120.35 mL of ethanol, and 115.65 mL of ammonium hydroxide. This mixture was stirred for 15 min. Sequentially, 17.25 mL of TEOS was added, maintaining stirring for 60 min at 30 °C. After this, nickel nitrate was added to the system and stirred for over 60 min. The obtained gel was filtered by gravity filtration using 500 mL of distilled water and over-dried at 60 °C for 48 h—adapted from Cazula et al. [26] and Zhuang et al. [27].

2.2. Preparation of Granulated Catalysts

To prepare the granulated catalysts, the methodology proposed by Oliveira et al. [28] was followed. The synthesized catalysts were first ground using a ball mill until the particles could pass through 355 to 500 µm sieves. Afterward, the sample was added to a muffle furnace with a programmed heating ramp: (1) heating at 3 °C min^{-1} to 200 °C, holding for 240 min; (2) heating at 3 °C min^{-1} to 280 °C, holding for 240 min; (3) heating at 3 °C min^{-1} to 400 °C, holding for 240 min; (4) heating at 3 °C min^{-1} to 520 °C, holding for 360 min; and heating at 5 °C min^{-1} to 800 °C, holding for 240 min [15,16].

The granulation method utilized was based on Zempulski et al. [29], with the addition of 2% (*w*/*w*) magnesium stearate ($Mg(C_{18}H_{35}O_2)_2$) (Sigma Aldrich, Barueri, SP, Brazil, ≥90%) to the powdered catalyst as a binder. The powder blend was placed into a 9 mm diameter cylindrical chamber of a stainless-steel mold, and a pressure of 159 MPa was applied using a manual hydraulic press. This process formed pellets approximately 9 mm in diameter and 2 mm in height, which were subsequently calcined in a muffle furnace at 400 °C for 30 min, with a heating rate of 20 °C min^{-1}. After calcination, the pellets were disaggregated using a mortar, and pestle and sieved to obtain granules in the 355–500 µm size range [28].

2.3. Catalytic Efficiency in DR

DR reaction experiments were applied using the catalysts obtained, to assess their efficiency to produce syngas. The catalyst was packed into a fixed-bed reactor and purged with N_2 (purity > 99.999%—White Martins, Maringá, PR, Brazil) for 30 min. Then, it was activated in situ with H_2 at 40 mL min^{-1} for 4 h, using a gas preheating system kept at 650 °C maintaining the catalyst at 800 °C. Another 30 min N_2 purge to remove any residual gas was carried out. The reaction was performed for 6 h, using a synthetic biogas flux, in proportions of 52% CH_4 and 48% CO_2, with a flow rate of 17.0 mL s^{-1}.

The gaseous products were analyzed using a gas chromatograph (DynamiQ-S-micro CG—QMICRO, Nova Analítica, Diadema, SP, Brazil) equipped with a nano-TCD detector. A chromatographic column type PLOT MS5A and a U-bond column were used. The carrier gas used was Ar (high purity > 99.999%—White Martins, Maringá, PR, Brazil).

The conversions of CH_4 and CO_2, as well as the molar fractions of H_2 and CO, were determined following the equations below [30,31].

$$\%CO_{2(\text{conversion})} = \frac{nCO_{2\text{in}} - nCO_{2\text{out}}}{nCO_{2\text{in}}} \times 100 \quad (2)$$

$$\%CH_{4(\text{conversion})} = \frac{nCH_{4\text{in}} - nCH_{4\text{out}}}{nCH_{4\text{in}}} \times 100 \quad (3)$$

$$F_i = \frac{n_{i\ \text{out}}}{(nCH_4 + nCO_2 + nH_2 + nCO)_{\text{out}}} \quad (4)$$

In which n is the number of moles, and F_i is the molar fraction of the gases.

2.4. Catalysts Characterization

Both catalysts, A and B, were characterized regarding their morphological, textural, and physical–chemical properties. N_2 physisorption analyses were performed using a Quantachrome Nova 2000e Instrument (Anton Paar QuantaTec, Boynton Beach, FL, EUA), with a relative pressure range between 0.05 and 0.95, at a temperature of 77 K. The specific surface area, pore volume, and pore size of the catalysts were determined using the BET (Brunauer–Emmett–Teller), BJH (Barrett–Joyner–Halenda), and DH (Dollimore–Heal) methods [20–22]. The samples were degassed in a vacuum system at 150 °C for 3 h.

The morphology of the catalysts was evaluated using a Scanning Electron Microscope (SEM-FEI-Quanta 440, Anton Paar QuantaTec, Boynton Beach, FL, EUA). The samples were first dried at 100 °C in an oven for 24 h to remove humidity and then submitted for analysis, by sputtering and scattering modules. Transmission Electron Microscopy (TEM) was also performed. The images were captured using an FEI TECNAI G2 F20 transmission electron microscope (Jeol USA Inc., Peabody, MA, USA). Experiments were performed under vacuum conditions (about 10^{-5} Pa) and high voltage (200 kV).

X-ray diffraction (XRD) was performed for the catalysts, A and B, before the DR reaction. The analyses were made in a Bruker diffractometer, model D2-PHASER (Bruker, Billerica, MA, EUA), using catalyst samples with granulometry below 106 µm. Bragg angles were taken by range from 0.5 to 80°, with Cu Kα radiation (λ = 1.5418 Å) and nickel filter, with a voltage of 30 kV, electrical current of 10 mA, and continuous scan of 0.02 min^{-1} of the 2θ with a time step of 1.0 s.

Programmed Temperature Reduction (TPR) was conducted using Altamira Instruments-AMI 300EZ (Altamira Instruments, Cumming, GA, USA) equipment equipped with a TCD detector, in which 25 mg of the catalyst sample was placed inside a quartz tube and initially treated with Ar (40 mL min^{-1}) at 500 °C. Sequentially, the sample was subjected to a reducing atmosphere using a mixture of 10% of H_2/Ar, and the temperature was increased from 50 to 900 °C.

3. Results and Discussion

3.1. Catalysts Characterization

Table 1 presents the textural parameters obtained for the produced catalysts using two different stages for Ni addition (before and after adding silica source). From the results presented in Table 1, it can be observed that catalyst A (Ni/Si-MCM-41-A) presented a surface area of 204.27 m^2 g^{-1}, which is 49% lower than obtained for B (Ni/Si-MCM-41-B).

This result could be attributed to the stage at which Ni was introduced to the synthesis. For catalyst B, Ni was added after the structure-directing agent, enhancing the formation of an ordered catalytic structure and promoting a more effective mesoporous development, thereby increasing the catalyst's surface area. Figure 1 proposes a mechanism for both cases, with metal acting separately or together with the mesoporous structure-directing agent.

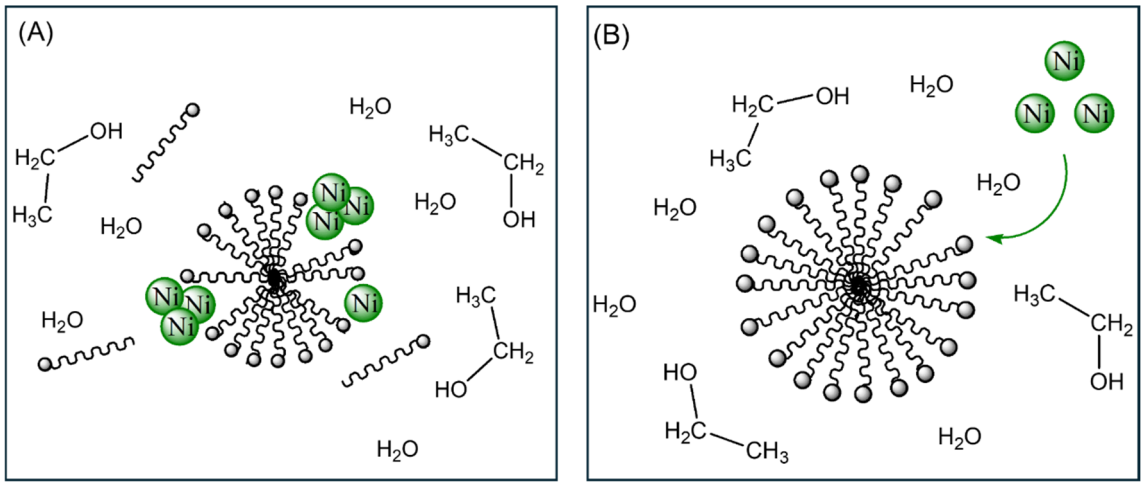


Figure 1. The Proposed mechanism for forming the mesoporous structure of catalysts A (**A**) and B (**B**), based on and adapted from Cazula et al. [26].

By analyzing the pore volume displayed in Table 1, A exhibited a smaller pore volume (0.05 cm^3 g^{-1}), while B showed a significantly larger pore volume (0.30 cm^3 g^{-1})—83% higher. According to Wen et al. [32], this structural aggregation may result in lower specific surface areas of catalysts. In this sense, the lowest surface area obtained for catalyst A can be explained by the interaction between nickel ions inside the pores and the structure-directing agent (silica source, i.e., TEOS). Compared to catalyst B, the lower pore volume observed for catalyst A supports the hypothesis that Ni directly influences the development of the material's porous structure.

Table 1. Textural parameters for catalysts A and B.

Catalyst	Surface Area (m^2 g^{-1})	Total Pore Volume (cm^3 g^{-1})	Pore Size (Å)
A	204.27	0.058	16.38
B	412.56	0.309	18.31

Figure 2 shows the N_2 adsorption–desorption isotherms obtained for the catalysts. The pore size distribution for these materials can be observed in Figure 3.

The N_2 adsorption–desorption isotherms observed in the synthesized catalysts are classified as type IV, characteristic of mesoporous materials. The hysteresis loops, more intense for B, identified as type H1, are typical of solids with a narrow distribution of uniform mesopores as found in templated silica materials like MCM-41 [25]. This indicates a well-defined and consistent mesoporous framework in catalyst B.

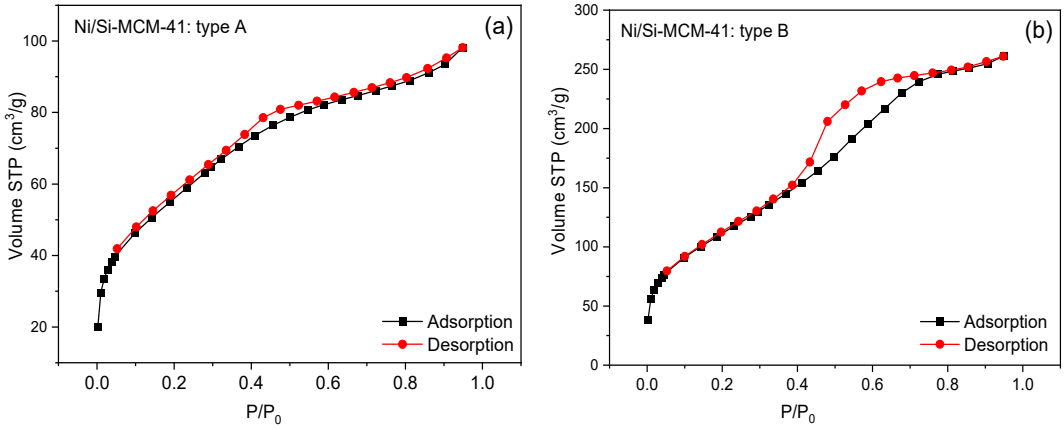


Figure 2. N_2 adsorption–desorption isotherms for catalysts A (**a**) and B (**b**).

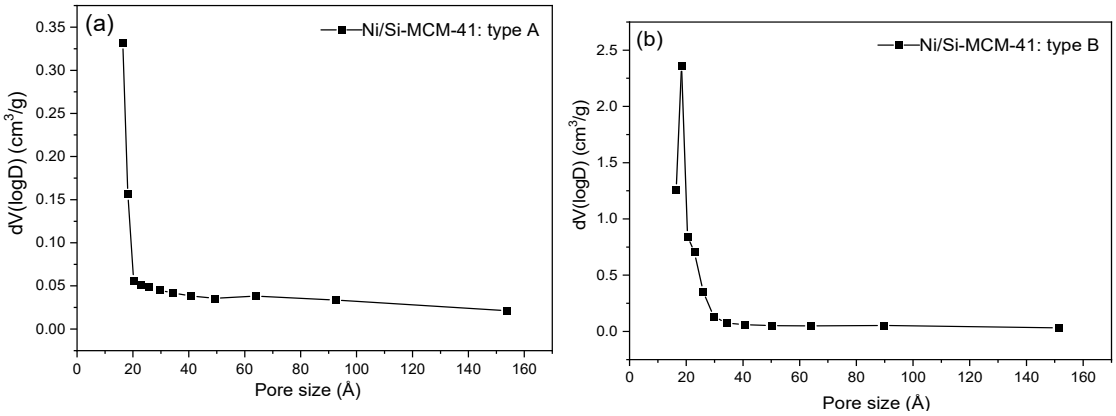


Figure 3. Pore size distribution for catalysts A (**a**) and B (**b**).

Figure 4 shows SEM images for the synthesized catalysts, where the morphological structure of the materials can be seen.

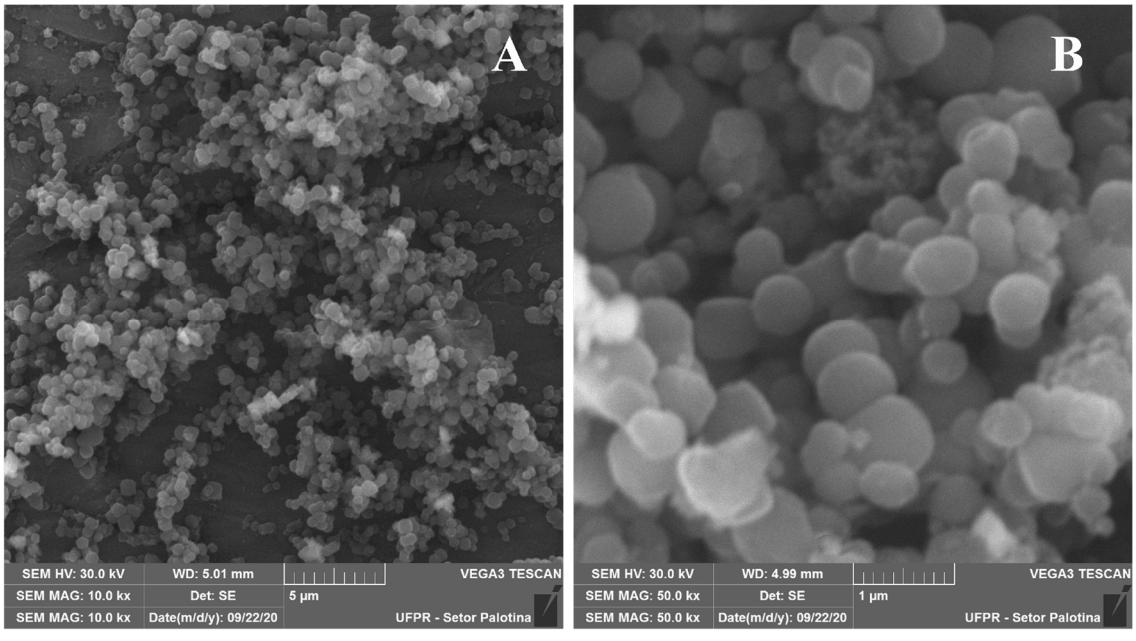


Figure 4. *Cont.*

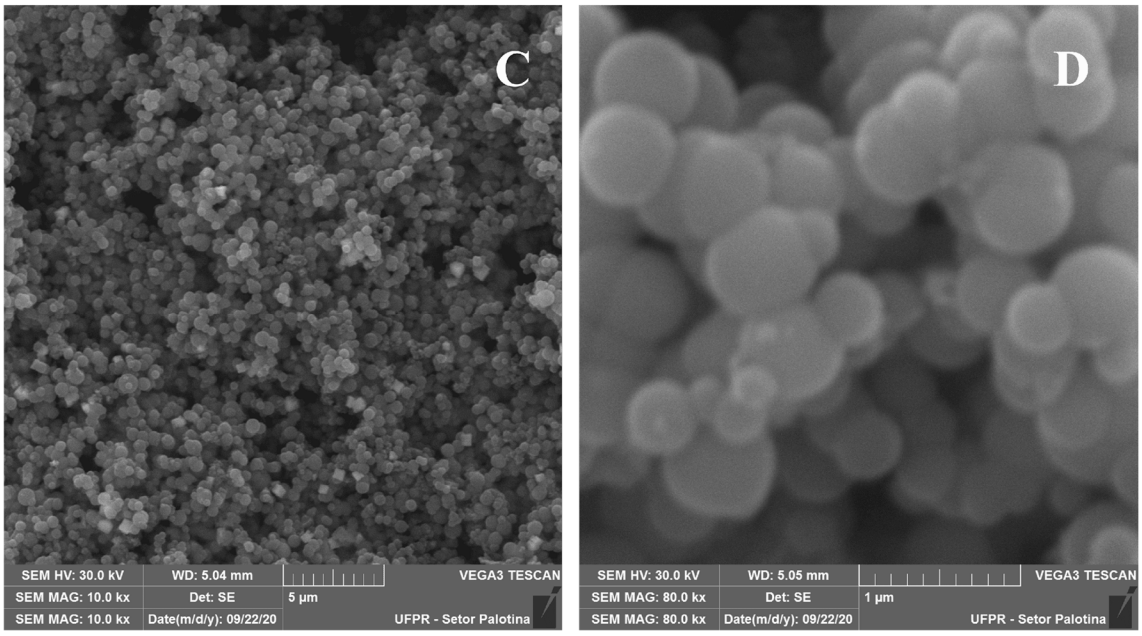


Figure 4. SEM analyses for catalyst A (**A**,**B**) and B (**C**,**D**).

According to Figure 4, the morphology of both catalysts is characterized by homogeneous spherical particles, typical for mesoporous MCM-41 materials. Additionally, Figure 4D reveals smaller irregular particles, which are attributed to metallic Ni on the catalyst surface. This phenomenon is primarily due to the migration of nickel ions from inside the pores to the surface during calcination [24]

TEM images, in Figure 5, reveal Ni particles on the catalyst's surface. Additionally, the differences between the formation of metallic structures in the studied catalysts can be observed.

Catalyst A exhibits a crystalline metallic structure with large particle aggregates on its surface. Meanwhile, for catalyst B, the metal is dispersed throughout, leading to the formation of filamentous Ni structures spread uniformly across the catalyst surface.

Both catalysts demonstrate the presence of an active metallic phase capable of effectively promoting DR, although with differing morphologies. In catalyst A, despite its less mesoporous characteristic, the robust and crystalline nickel formations are expected to contribute significantly to its high conversion performance, while catalyst B, with its well-defined mesoporous structure and more uniform dispersion of smaller nickel particles, is anticipated to achieve high reaction conversions, even though its active phase tends to be more amorphous [24].

The temperature-programmed reduction (TPR) profiles for A (Figure 6a) and B (Figure 6b) show significant differences. For A, two distinct peaks were observed at 540 °C and 765 °C. In contrast, catalyst B exhibited a prominent peak at 565 °C with an additional shoulder-like peak around 800 °C. The reduction peak at 540 °C in Ni/MCM-41 A is attributed to bulk NiO reduction, while the reduction at a higher temperature (765 °C) indicates a strong bonding between NiO particles and the MCM-41 structure. In catalyst B, the reduction peak shifts to 565 °C with a wider peak ranging from 360 to 800 °C.

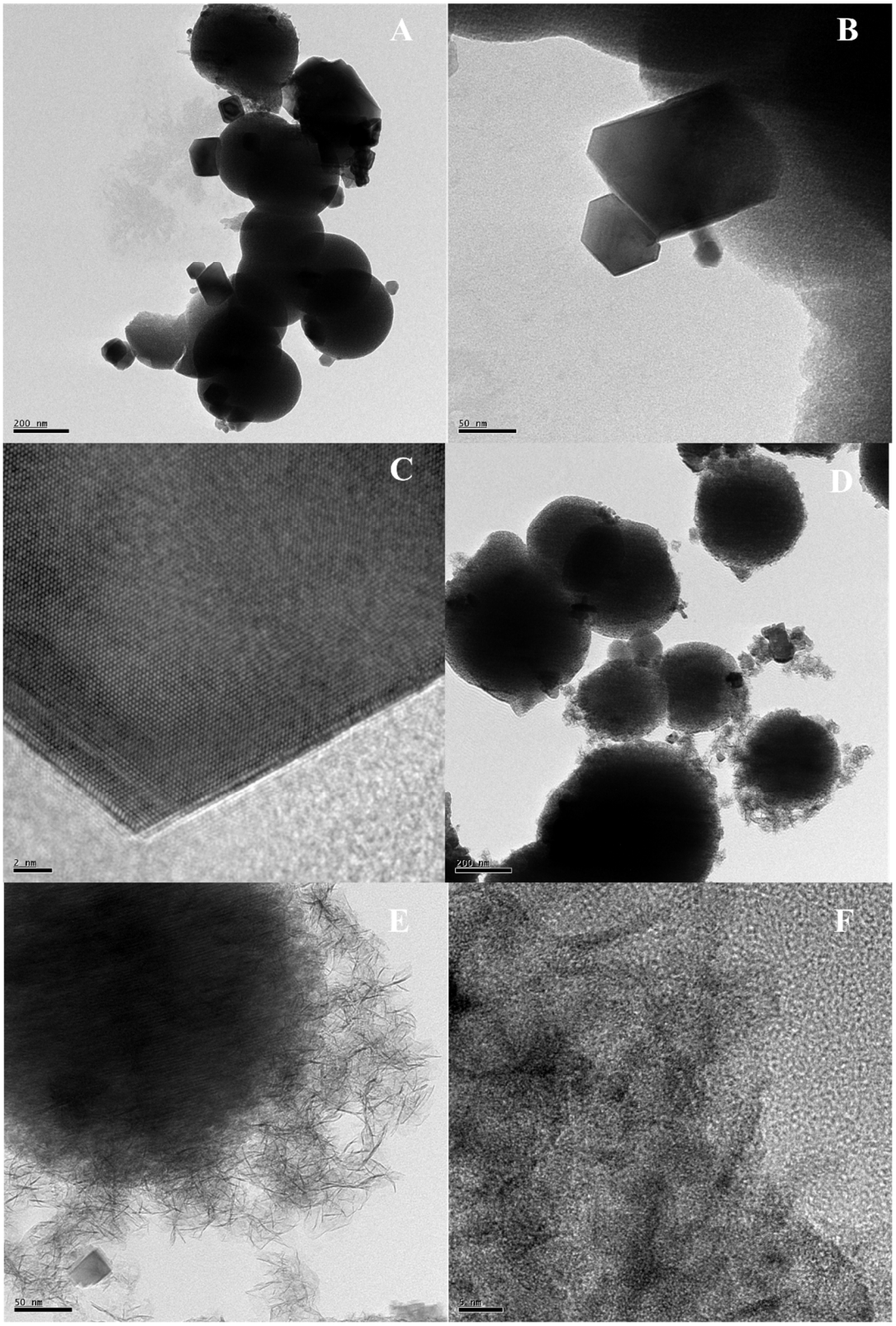


Figure 5. TEM images for catalyst A (**A**–**C**) and B (**D**–**F**). Images were obtained at high resolution and different magnifications.

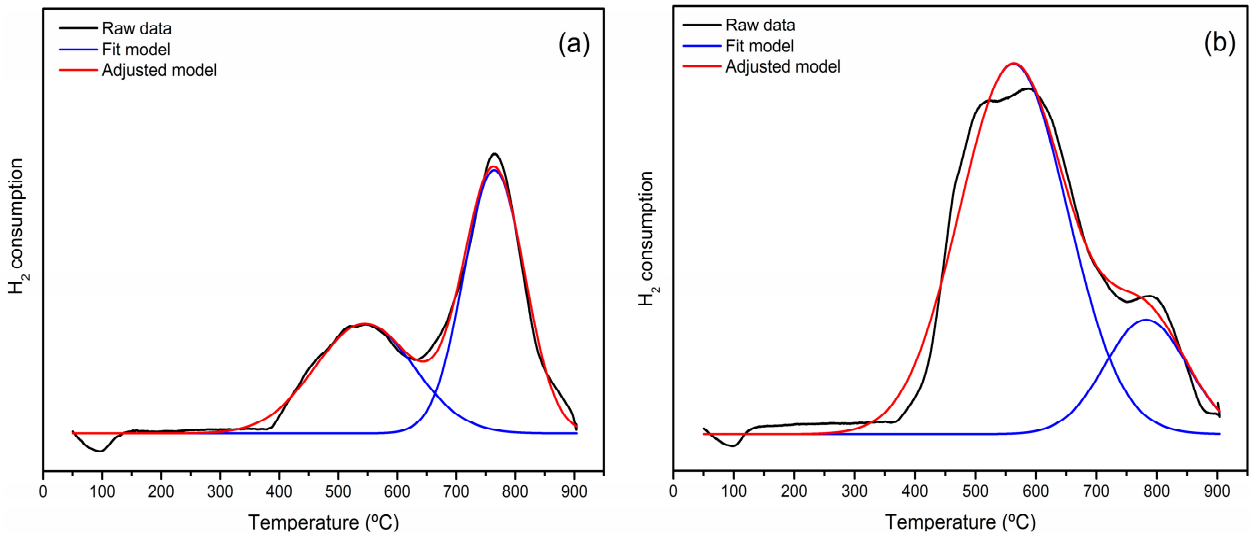


Figure 6. Temperature programmed reduction (TPR) analyses for catalyst A (**a**) and B (**b**).

According to Afzal et al. [33], broader peaks, such as those observed in catalyst B, suggest stronger metal–support interactions. Considering the obtained profiles, it is possible to indicate that NiO from B is more tightly bound to the support compared to nickel in catalyst A, which also exhibits strong binding regions but to a lesser extent [34,35].

The results of the XDR analysis are available in Figure 7, for both catalysts (A and B), before their performances through DR, as indicated. Is possible to notice, in the diffractograms for the catalysts before DR, the presence of the typical peaks for NiO close to 37, 43, 63, and 75° 2θ, corresponding to the (111), (200), (220), and (311) planes, respectively. This observation indicates the nickel oxide in the face-centered cubic phase (JCPDS47-1049), indicating, along with the efficient deposition of nickel on the catalyst, that the calcination process was completed.

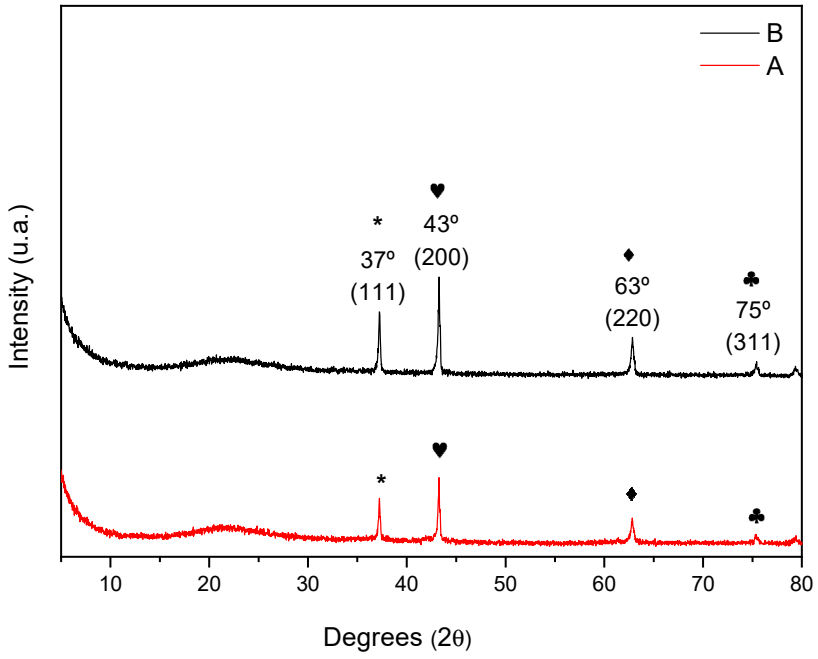


Figure 7. XDR obtained before and after the catalysts' performance on DR. The icons—*, ♥, ◆, ♣—correspond to the angles and planes of the diffractograms, indicating that both catalysts presented the same properties.

3.2. Dry Reforming Results

Figure 8 presents molar fractions of gaseous products formed during DR reaction tests. Both catalysts exhibited low concentrations of CH_4 and CO_2 and high values for gas conversions (superior to 95%). The average molar fraction of H_2 was 44% for the catalysts; however, B showed better stability during the DR, certainly due to its better textural parameters and morphological aspects along with the greater bound strength between Ni and support.

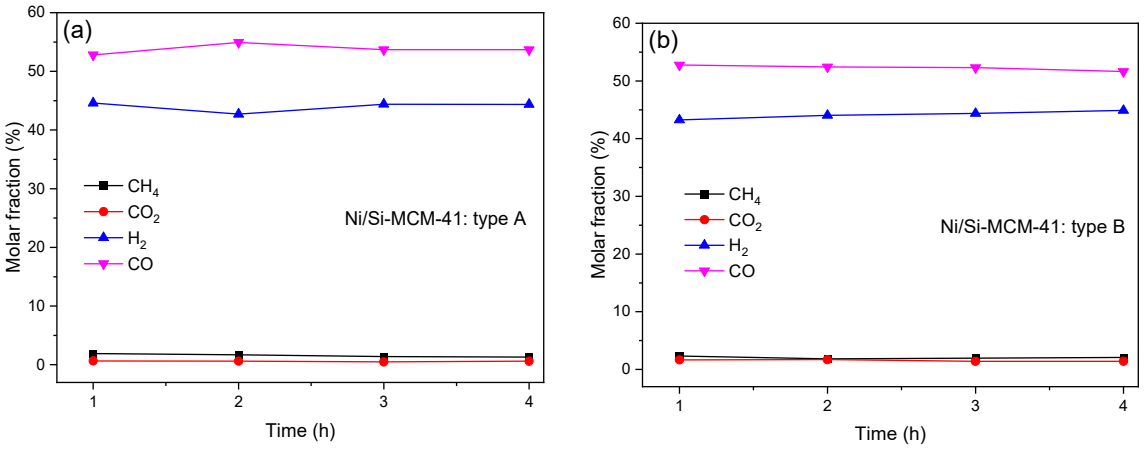


Figure 8. The molar fraction of the products obtained from DR tests with catalysts A (**a**) and B (**b**).

The catalysts synthesized were effective in converting biogas into syngas and H_2, indicating that both synthesis processes were effective in obtaining high-performance catalysts. For A, the simultaneous metal phase addition stage technique used offered notable benefits, such as the simplification of the conventional process commonly described in the literature—wet impregnation, for B. Consequently, it can be concluded that changing the Ni addition stages did not compromise the catalytic efficiency of the material compared to significant recent studies from the research group available in the literature [24,28].

For comparison with the state of the art, Table 2 summarizes the parameters for DR: comparison of surface area, catalyst mass, CH_4 conversion, and H_2/CO molar ratio, between the literature reported and the presented work. Research involving catalysts with a variety of metals and supports are presented. The studies evidence conversions above 70% and an H_2/CO molar ratio above 0.5. In this work, the catalysts provided conversions of 97% and 96% for Ni/SiMCM-41_A and Ni/SiMCM-41_B, respectively. The H_2/CO could be also comparable, positioning A and B as efficient alternatives, especially in terms of structural properties. The results of this work reveal that, even with the modified synthesis, the catalyst can be promising in the conversion process through DR. The reactor type is selected according to the resistance of the materials concerning the high reaction temperature. It is also important to understand the complexity of choosing catalysts for DR. It is important to emphasize that in this way, optimization in catalyst synthesis is promising and can reduce the impacts of its synthesis and still maintain process efficiency.

Table 2. Parameters in DR: comparison of surface area, catalyst mass, and conversion between the literature and the presented work.

Catalyst	Surface Area (m^2/g)	Reactor	Temperature (°C)	Catalyst Mass (g)	CH_4 Conversion (%)	H_2/CO	Reference
Sr/Ni/MCM-41	212.3	quartz	700	0.2	73.3	0.88	Estalkhi et al., 2024 [36]
10Ni/SBA-15	592	stainless steel	700	0.05	70.4	0.85	Chotirach et al., 2018 [37]
5Ni2Mg3SiAl	230.15	stainless steel	700	0.10	86	0.95	Bagabas et al., 2021 [38]
Co–Ru–Zr/SiO_2 Co–Ru–Zr/γ-Al_2O_3 Co–Ru–Zr/MgO	108.4 126.9 36.82	quartz	800	0.2	90 92 80	0.90 0.91 0.87	Lee et al., 2014 [39]
Cs-Ni/FSA	152.74	stainless steel	850	0.2	93	0.5	Owgi et al., 2023 [40]
Ni@S-1@SiO_2	630	quartz	800	0.05	93.7	-	Li et al., 2024 [41]
5%Ni/La2O3-KIT-6	55.3	quartz	700	0.1	~70	~0.8	Song et al., 2021 [42]
2Y_2O_3–NiO/MgO-MCM-41	445.7	quartz	750	0.2	79	0.85	Taherian et al., 2020 [43]
This work							
Ni/SiMCM-41_A	204.2	stainless steel	800	3	97	0.82	
Ni/SiMCM-41_B	412.5	stainless steel	800	3	96	0.84	

4. Conclusions

It can be concluded that a Ni addition stage in the catalyst structure, before and after the formation of the mesoporous structure, aiming to exclude the wet impregnation step in the synthesis of Ni catalysts supported on MCM-41, was efficient, resulting in conversions exceeding 95%. The greatest differences between the structures formed for the catalysts, A and B, could be observed in the morphological characterization results, which showed that the Ni addition stage, before the silica source—TEOS—leads to the formation of a less porous structure with a smaller surface area and in which the Ni particles form crystalline clusters on the catalyst surface. However, the metal addition stage did not correlate with a significant increase or decrease in the efficiency of the catalysts when applied to DR, for converting biogas into renewable hydrogen, since the conversion results were 97% and 96% for Ni/SiMCM-41_A and Ni/Si-MCM-41_B, respectively.

Author Contributions: Conceptualization, H.J.A.; Data curation, C.T.d.N. and B.B.C.; Investigation, L.G.O., A.T., C.d.J.d.O., G.E.Q.S., L.J.G., Á.d.O.A., G.R. and N.N.J.; Methodology, L.G.O.; Project administration, H.J.A.; Resources, H.J.A.; Supervision, H.J.A.; Writing—original draft, L.G.O.; Writing—review and editing, C.T.d.N., B.B.C. and H.J.A. All authors have read and agreed to the published version of the manuscript.

Funding: This research received no external funding.

Data Availability Statement: Data are contained within the article, further inquiries can be directed to the corresponding author.

Acknowledgments: This work has been supported by the 'CNPq' through CNPQ-PQ-305480/2019-7, MAI-DAI 140466/2021-5, and CNPq-PQ-305433/2022-9; and by the "Fundação Araucária" through CONVÊNIO PD&I 307/2023—NAPI Hidrogênio; are gratefully acknowledged.

Conflicts of Interest: The authors declare no conflict of interest.

References

1. Bairrão, D.; Soares, J.; Almeida, J.; Franco, J.F.; Vale, Z. Green Hydrogen and Energy Transition: Current State and Prospects in Portugal. *Energies* **2023**, *16*, 551. [CrossRef]
2. Espegren, K.; Damman, S.; Pisciella, P.; Graabak, I.; Tomasgard, A. The Role of Hydrogen in the Transition from a Petroleum Economy to a Low-Carbon Society. *Int. J. Hydrogen Energy* **2021**, *46*, 23125–23138. [CrossRef]
3. Delparish, A.; Avci, A.K. Intensified Catalytic Reactors for Fischer-Tropsch Synthesis and for Reforming of Renewable Fuels to Hydrogen and Synthesis Gas. *Fuel Process. Technol.* **2016**, *151*, 72–100. [CrossRef]
4. Aravindan, M.; Hariharan, V.S.; Narahari, T.; Kumar, A.; Madhesh, K.; Kumar, P.; Prabakaran, R. Fuelling the Future: A Review of Non-Renewable Hydrogen Production and Storage Techniques. *Renew. Sustain. Energy Rev.* **2023**, *188*, 113791. [CrossRef]
5. Amin, M.; Shah, H.H.; Fareed, A.G.; Khan, W.U.; Chung, E.; Zia, A.; Rahman Farooqi, Z.U.; Lee, C. Hydrogen Production through Renewable and Non-Renewable Energy Processes and Their Impact on Climate Change. *Int. J. Hydrogen Energy* **2022**, *47*, 33112–33134. [CrossRef]
6. Zhang, K.; Jin, Z.; Liu, Q.; Liu, L. Novel Green Hydrogen—Fossil Fuel Dehydrogenation. *Fundam. Res.* **2024**. [CrossRef]
7. Ishaq, H.; Dincer, I.; Crawford, C. A Review on Hydrogen Production and Utilization: Challenges and Opportunities. *Int. J. Hydrogen Energy* **2022**, *47*, 26238–26264. [CrossRef]
8. Guan, D.; Wang, B.; Zhang, J.; Shi, R.; Jiao, K.; Li, L.; Wang, Y.; Xie, B.; Zhang, Q.; Yu, J.; et al. Hydrogen Society: From Present to Future. *Energy Environ. Sci.* **2023**, *16*, 4926–4943. [CrossRef]
9. Abdin, Z.; Zafaranloo, A.; Rafiee, A.; Mérida, W.; Lipiński, W.; Khalilpour, K.R. Hydrogen as an Energy Vector. *Renew. Sustain. Energy Rev.* **2020**, *120*, 109620. [CrossRef]
10. Nikolaidis, P.; Poullikkas, A. A Comparative Overview of Hydrogen Production Processes. *Renew. Sustain. Energy Rev.* **2017**, *67*, 597–611. [CrossRef]
11. Acar, C.; Dincer, I. Review and Evaluation of Hydrogen Production Options for Better Environment. *J. Clean. Prod.* **2019**, *218*, 835–849. [CrossRef]
12. Fernandes, D.J.; Ferreira, A.F.; Fernandes, E.C. Biogas and Biomethane Production Potential via Anaerobic Digestion of Manure: A Case Study of Portugal. *Renew. Sustain. Energy Rev.* **2023**, *188*, 113846. [CrossRef]
13. Abatzoglou, N.; Boivin, S. A Review of Biogas Purification Processes. *Biofuels Bioprod. Biorefining* **2009**, *3*, 42–71. [CrossRef]
14. Hajizadeh, A.; Mohamadi-Baghmolaei, M.; Cata Saady, N.M.; Zendehboudi, S. Hydrogen Production from Biomass through Integration of Anaerobic Digestion and Biogas Dry Reforming. *Appl. Energy* **2022**, *309*, 118442. [CrossRef]

15. EPE (Empresa de Pesquisa Energética). Análise de Conjuntura Dos Biocombustíveis. 2021. Available online: https://www.epe.gov.br/sites-pt/publicacoes-dados-abertos/publicacoes/PublicacoesArquivos/publicacao-688/NT-EPE-DPG-SDB-2022-02_Analise_de_Conjuntura_dos_Biocombustiveis_2021.pdf (accessed on 20 July 2024).
16. Gao, Y.; Jiang, J.; Meng, Y.; Yan, F.; Aihemaiti, A. A Review of Recent Developments in Hydrogen Production via Biogas Dry Reforming. *Energy Convers. Manag.* **2018**, *171*, 133–155. [CrossRef]
17. Al-Fatesh, A.S.; Atia, H.; Abu-Dahrieh, J.K.; Ibrahim, A.A.; Eckelt, R.; Armbruster, U.; Abasaeed, A.E.; Fakeeha, A.H. Hydrogen Production from CH_4 Dry Reforming over Sc Promoted Ni/MCM-41. *Int. J. Hydrogen Energy* **2019**, *44*, 20770–20781. [CrossRef]
18. Jung, S.; Lee, J.; Moon, D.H.; Kim, K.-H.; Kwon, E.E. Upgrading Biogas into Syngas through Dry Reforming. *Renew. Sustain. Energy Rev.* **2021**, *143*, 110949. [CrossRef]
19. Abdulrasheed, A.; Jalil, A.A.; Gambo, Y.; Ibrahim, M.; Hambali, H.U.; Shahul Hamid, M.Y. A Review on Catalyst Development for Dry Reforming of Methane to Syngas: Recent Advances. *Renew. Sustain. Energy Rev.* **2019**, *108*, 175–193. [CrossRef]
20. Zhang, J.; Li, F. Coke-Resistant Ni@SiO_2 Catalyst for Dry Reforming of Methane. *Appl. Catal. B* **2015**, *176–177*, 513–521. [CrossRef]
21. Zhang, J.; Xin, Z.; Meng, X.; Tao, M. Synthesis, Characterization and Properties of Anti-Sintering Nickel Incorporated MCM-41 Methanation Catalysts. *Fuel* **2013**, *109*, 693–701. [CrossRef]
22. Abdelhamid, H.N. A Review on Hydrogen Generation from the Hydrolysis of Sodium Borohydride. *Int. J. Hydrogen Energy* **2021**, *46*, 726–765. [CrossRef]
23. Aguiar, M.; Cazula, B.B.; Saragiotto Colpini, L.M.; Borba, C.E.; Alves da Silva, F.; Noronha, F.B.; Alves, H.J. Si-MCM-41 Obtained from Different Sources of Silica and Its Application as Support for Nickel Catalysts Used in Dry Reforming of Methane. *Int. J. Hydrogen Energy* **2019**, *44*, 32003–32018. [CrossRef]
24. Cazula, B.; da Fonseca, R.; Marinho, A.L.; Noronha, F.; Arroyo, P.A.; Yamamoto, C.; Brackmann, R.; José Alves, H. Performance Study of Ni/Si-MCM-41 Catalysts, Synthesized with Different Silica Sources, and Their Application on Methane Dry Reform to Produce Green Hydrogen. *J. Braz. Chem. Soc.* **2024**, *35*, e-20230133. [CrossRef]
25. Grün, M.; Unger, K.K.; Matsumoto, A.; Tsutsumi, K. Novel Pathways for the Preparation of Mesoporous MCM-41 Materials: Control of Porosity and Morphology. *Microporous Mesoporous Mater.* **1999**, *27*, 207–216. [CrossRef]
26. Cazula, B.B.; Oliveira, L.G.; Machado, B.; Alves, H.J. Optimization of Experimental Conditions for the Synthesis of Si-MCM-41 Molecular Sieves Using Different Methods and Silica Sources. *Mater. Chem. Phys.* **2021**, *266*, 124553. [CrossRef]
27. Zhuang, J.; Yan, S.; Zhang, P.; Liu, X.; Zhao, Y.; Yu, Y.; Wang, Y.; Zhao, Q.; Wu, H.; Zhu, X.; et al. Regulating the States of Ni Species by Controlling the Silanols of MCM-41 Support to Promote the Hydrogenation of Maleic Anhydride. *Fuel* **2023**, *335*, 127030. [CrossRef]
28. Oliveira, L.G.; Machado, B.; Pereira de Souza, L.; Gosch Corrêa, G.C.; Polinarski, M.A.; Cavalcanti Trevisan, S.V.; Borba, C.E.; Brackmann, R.; Alves, H.J. Dry Reforming of Biogas in a Pilot Unit: Scale-up of Catalyst Synthesis and Green Hydrogen Production. *Int. J. Hydrogen Energy* **2022**, *47*, 35608–35625. [CrossRef]
29. Zempulski, D.A.; Postaue, N.; Stevanato, N.; Alves, H.J.; Silva, C. Study of the Operational Conditions for Ethyl Esters Production Using Residual Frying Oil and KF/Clay Catalyst in a Continuous System. *Grasas y Aceites* **2022**, *73*, e453. [CrossRef]
30. Ayodele, B.V.; Khan, M.R.; Cheng, C.K. Catalytic Performance of Ceria-Supported Cobalt Catalyst for CO-Rich Hydrogen Production from Dry Reforming of Methane. *Int. J. Hydrogen Energy* **2016**, *41*, 198–207. [CrossRef]
31. Charisiou, N.D.; Siakavelas, G.; Papageridis, K.N.; Baklavaridis, A.; Tzounis, L.; Avraam, D.G.; Goula, M.A. Syngas Production via the Biogas Dry Reforming Reaction over Nickel Supported on Modified with CeO_2 and/or La_2O_3 Alumina Catalysts. *J. Nat. Gas Sci. Eng.* **2016**, *31*, 164–183. [CrossRef]
32. Wen, T.; Zhao, Y.; Jiao, X.; Zhang, Q.; Zhang, T.; Zhang, X.; Qu, J.; Dong, Y.; Song, S. High-Performance Nickel/Iron Catalysts for Oxygen Evolution in PH-near-Neutral Borate Electrolyte Synthesized by Mechanochemical Approach. *J. Alloys Compd.* **2022**, *898*, 162845. [CrossRef]
33. Afzal, M.; Theocharis, C.R.; Karim, S. Temperature Programmed Reduction of Silica Supported Nickel Catalysts. *Colloid Polym. Sci.* **1993**, *271*, 1100–1105. [CrossRef]
34. Li, Y.; Wang, J.; Ding, C.; Ma, L.; Xue, Y.; Guo, J.; Wang, S.; Meng, Y.; Zhang, K.; Liu, P. Effect of Cobalt Addition on the Structure and Properties of Ni–MCM-41 for the Partial Oxidation of Methane to Syngas. *RSC Adv.* **2019**, *9*, 25508–25517. [CrossRef] [PubMed]
35. Ding, C.; Wang, J.; Li, Y.; Ma, Q.; Ma, L.; Guo, J.; Ma, Z.; Liu, P.; Zhang, K. The Role of Active Sites Location in Partial Oxidation of Methane to Syngas for MCM-41 Supported Ni Nanoparticles. *Catalysts* **2019**, *9*, 606. [CrossRef]
36. Hasani Estalkhi, M.; Yousefpour, M.; Koohestan, H.; Taherian, Z. Catalytic Evaluation of Ni–3%Sr-/MCM-41 in Dry and Steam Reforming of Methane. *Int. J. Hydrogen Energy* **2024**, *68*, 1344–1351. [CrossRef]
37. Chotirach, M.; Tungasmita, S.; Nuntasri Tungasmita, D.; Tantayanon, S. Titanium Nitride Promoted Ni-Based SBA-15 Catalyst for Dry Reforming of Methane. *Int. J. Hydrogen Energy* **2018**, *43*, 21322–21332. [CrossRef]
38. Bagabas, A.; Al-Fatesh, A.S.; Kasim, S.O.; Arasheed, R.; Ibrahim, A.A.; Ashamari, R.; Anojaidi, K.; Fakeeha, A.H.; Abu-Dahrieh, J.K.; Abasaeed, A.E. Optimizing MgO Content for Boosting γ-Al_2O_3-Supported Ni Catalyst in Dry Reforming of Methane. *Catalysts* **2021**, *11*, 1233. [CrossRef]
39. Lee, J.-H.; You, Y.-W.; Ahn, H.-C.; Hong, J.-S.; Kim, S.-B.; Chang, T.-S.; Suh, J.-K. The Deactivation Study of Co–Ru–Zr Catalyst Depending on Supports in the Dry Reforming of Carbon Dioxide. *J. Ind. Eng. Chem.* **2014**, *20*, 284–289. [CrossRef]

40. Owgi, A.H.K.; Jalil, A.A.; Aziz, M.A.A.; Alhassan, M.; Hambali, H.U.; Nabgan, W.; Saravanan, R.; Hatta, A.H. Effect of Promoters (Ce, Sr, Cs, and Sm) on the Activity and Coke Formation of FSA Support Ni in the Dry Reforming of Methane. *Fuel* **2023**, *340*, 127592. [CrossRef]
41. Li, M.; Liu, W.; Mao, Y.; Liu, K.; Zhang, L.; Cao, Z.; Ma, Q.; Ye, L.; Peng, H. Design Dual Confinement Ni@S-1@SiO_2 Catalyst with Enhanced Carbon Resistance for Methane Dry Reforming. *Int. J. Hydrogen Energy* **2024**, *83*, 79–88. [CrossRef]
42. Song, J.; Duan, X.; Zhang, W. Methane Dry Reforming over Mesoporous La_2O_3 Supported Ni Catalyst for Syngas Production. *Microporous Mesoporous Mater.* **2021**, *310*, 110587. [CrossRef]
43. Taherian, Z.; Khataee, A.; Orooji, Y. Facile Synthesis of Yttria-Promoted Nickel Catalysts Supported on MgO-MCM-41 for Syngas Production from Greenhouse Gases. *Renew. Sustain. Energy Rev.* **2020**, *134*, 110130. [CrossRef]

Disclaimer/Publisher's Note: The statements, opinions and data contained in all publications are solely those of the individual author(s) and contributor(s) and not of MDPI and/or the editor(s). MDPI and/or the editor(s) disclaim responsibility for any injury to people or property resulting from any ideas, methods, instructions or products referred to in the content.